Journal of the European Ceramic Society 43 (2023) 1531–1541

Contents lists available at ScienceDirect

Journal of the European Ceramic Society

journal homepage: www.elsevier.com/locate/jeurceramsoc

The effect of liquid phase chemistry on the densification and strength of cold sintered ZnO

Abdullah Jabr [a], Julian Fanghanel [b,c,*], Zhongming Fan [c], Raul Bermejo [a,b], Clive Randall [b,c]

[a] Department of Materials Science, Montanuniversität Leoben, Franz Josef-Strasse 18, A-8700 Leoben, Austria
[b] Materials Science and Engineering Department, The Pennsylvania State University, University Park, PA 16802, USA
[c] Materials Research Institute, Millennium Science Complex, University Park , PA 16802, USA

ARTICLE INFO

Keywords:
Cold sintering
Densification
Strength
Formic acid
Zinc oxide

ABSTRACT

Cold sintering is a chemo-mechanical densification process which allows densification of ceramics at low temperatures below 300 °C. This substantial reduction in the sintering temperature is enabled by an externally applied pressure and a compatible transient liquid phase. In this paper, ZnO is cold sintered using various commercial organic acids: formic, acetic and citric acid. The effect of these different transient phases on densification, microstructural evolution and mechanical response is investigated. Fourier transform infrared spectroscopy, thermogravimetric analyses and transmission electron microscopy were conducted to explain the chemical interactions in the cold sintering process. High relative densities (~ 96 %) were achieved by formic and acetic acid, whereas poor densification was obtained for citric acid (< 80 %), despite the higher expected solubility of zinc oxide. The higher biaxial strength found in samples sintered with formic acid compared to acetic acid (i.e. ~90 MPa vs. ~40 MPa) is discussed supported by fractographic analyses.

1. Introduction

Ceramics are conventionally manufactured by thermal treatment of a shaped powder compact at temperatures in the range of 50–80 % of the melting point of the material. Since ceramics are characterized by a high melting point, these temperatures are usually higher than 1000 °C [1]. The use of such high temperatures results in deleterious effects such as thermal stresses, loss of volatile elements, reaction/diffusion between different phases, among other economical and environmental concerns related to energy consumption and carbon emissions. It is therefore desirable to be able to densify materials at low temperatures to avoid these effects. Furthermore, densification at low temperatures offers the co-integration of metals, polymers, and ceramics into unique dense composites, in ways not accessible by conventional bulk processing methods. Thus, lowering the sintering temperature of ceramics has been the incentive for developing new sintering techniques across broad families of ceramic materials and compositions. While the reduction in surface energy through thermal mass diffusion is the driving force in conventional sintering, alternative techniques, such as hot pressing, field-assisted sintering, microwave sintering [2] and liquid phase sintering, seek to activate densification at lower temperatures through application of external pressure [3], electric field [4] or addition of a liquid phase [5]. Although much progress has been achieved in reducing the sintering temperature, most of these techniques still operate at temperatures higher than those required for co-sintering of complex composite materials.

The cold sintering process (CSP) allows densification of ceramics at unprecedented low temperatures, below 300 °C [6]. This substantial reduction of the sintering temperature is enabled by an external pressure and a transient liquid phase, which provides a faster diffusion path for ionic and molecular species and drives mechanisms such as particle rearrangement, dissolution and precipitation [7–9]. The chemo-mechanical process that can drive these densification transport and precipitation mechanisms is known as pressure solution creep [10]. CSP has unlocked new design strategies and materials combinations which were previously unfeasible, such as co-integration of ceramics with polymers, nanomaterials and also metals. [11–13].

The mechanisms operating during cold sintering have been extensively studied on ZnO, commonly used as a model system in sintering studies. It has been shown that differences in chemistry of the transient solvent of the system can have a large effect on enabling the mechanism of pressure solution creep to take place. Funahashi et al. [9] densified ZnO to relative densities higher than 90 % using aqueous solution of acetic acid at temperatures well below 300 °C. However, no

* Corresponding author at: Materials Research Institute, Millennium Science Complex, University Park , PA 16802, USA.
E-mail address: juf624@psu.edu (J. Fanghanel).

https://doi.org/10.1016/j.jeurceramsoc.2022.11.071
Received 19 October 2022; Received in revised form 26 November 2022; Accepted 29 November 2022
Available online 1 December 2022

densification was achieved when pure water was used (only 65 % relative density), as ZnO is insoluble in water. These results indicated the importance of the solubility of the solid phase into the transient liquid phase. In this particular case, Zn^{2+} cations can diffuse from highly stressed contact areas with high chemical potential to pore surfaces with low chemical potential. This dissolution-precipitation step drives densification through the elimination of pores. Experiments by Kang et al. [14] showed that dissolution of ZnO into the liquid phase is not a prerequisite for cold sintering and that high densities (>98 %) can still be achieved if the liquid phase is presaturated with Zn^{2+} cations as in zinc acetate solution, albeit the pH value of 7, where ZnO is regarded as insoluble. Previous studies have reported an adverse effect of high acetic acid concentration in the liquid phase on densification in CSP of ZnO. Despite the higher dissolution capability, the reported densities were 88 % for 9 mol/L [15] and 70 % for 17.5 mol/L acetic acid [9], indicating the importance of the role of water in CSP. Sengul et al. [15] proposed a theoretical explanation of the role of water using Reactive force field modelling (ReaxFF). The model showed that water hydroxylates the surface of ZnO, forming bridging hydroxyl groups which facilitate the adsorption, diffusion, and hence, recrystallization of Zn^{2+} cations into ZnO. An excess of acetic acid would act as a diffusion barrier and occupy surface sites, which otherwise would have been available as recrystallization sites. Floyd et al. [16] investigated the effect of humidity on the CSP of ZnO using a solid transport phase of zinc acetate dihydrate containing only structural water. In their experiments, almost full densification was only achieved under processing conditions with more than 50 % relative humidity, demonstrating the role of small amounts of adsorbed water to drive mass transport through water-enhanced diffusion. The positive effect of small amounts of adsorbed water, despite being in the order of thin molecular layers, has been explained by enhanced particle packing due to the lubricating effect of the liquid film, enhanced cation adsorption and surface diffusion [15], and creation of diffusion pathways between the grains through defect formation [17]. Another important aspect is the interface reaction between the solid and liquid phase, as investigated in the experiments by Ndayishimiye et al. [18], where an aqueous solution of metal–organic chelate (zinc acetylacetonate hydrate) was used as a transient liquid phase. The result was ZnO with relative densities higher than 90 %. The proposed mechanism involved the hydrolysis of the chelate in water and its dynamic interaction with ZnO surfaces, leading to its precipitation onto ZnO. Nevertheless, this approach works for metal–organic chelates that have high propensity to transform into ZnO and exhibit fast hydrolysis.

Based on these investigations, several important factors associated with the role of the liquid phase for cold sintering ZnO can be deduced: a) the presence of water, b) the solubility of ZnO in the liquid phase to generate Zn^{2+} cations that can participate in the dissolution–precipitation step, or alternatively preloading the liquid phase with the cations, and c) a good chelating ability while maintaining low stability to promote back transformation to precipitate the ZnO. In this work, we propose an aqueous solution of formic acid as transient liquid phase for CSP, which meets all the mentioned requirements with the advantage of being the simplest organic acid with lowest carbon content. The aim of this study is to investigate the effect of liquid phase selection on densification, microstructure and mechanical response of cold sintered samples on the example of ZnO.

2. Experimental

2.1. Starting materials

All cold sintering experiments were performed on a commercial ZnO powder provided by Alfa Aesar (NanoArc™ ZN-0605) with a particle size between 40 and 100 nm. The transient liquid phases were prepared by diluting the acids to a concentration of 2 mol/L. This concentration was chosen based on a previous study by Bang et al. [19] showing enhanced kinetics at an acid concentration of 2 mol/L. In this study, the following acids were used: formic acid (reagent grade ≥95 %, Sigma-Aldrich®), acetic acid (glacial ≥ 99.7 %, VWR®) and citric acid (ACS reagent ≥ 99.0 %, Sigma-Aldrich®). For comparison, a cold sintered sample was prepared using deionized water as transient liquid phase.

2.2. Cold sintering process

First, 1 g of ZnO powder was mixed with 13 wt% of the respective liquid phase in an agate mortar and pestle. The mixed powder was then poured into a stainless-steel die with a diameter of 13 mm. Uniaxial pressure was applied using a semiautomated press (Enerpac®) equipped with an extensometer (Keyence GT2-H32), which is capable of monitoring vertical displacements with a 0.5 μm resolution. More details on the setup of the press can be found in [20]. Heat was applied using a mica band heater with a power of 300 W (Tempco®) wrapped around the die. The temperature was controlled by a PID controller connected to the band heater and a J-type thermocouple placed in the centre of a custom designed bottom base plate (see Ref. [19] for more details) of the die which measures the process temperature and provides feedback for the PID controller, see Fig. 1a. CSP started by applying 335 MPa uniaxial pressure at room temperature for 5 min, then heating to the target temperature with a heating rate of 5 °C/min. The dwell time for all experiments was 1 h and it only accounts for the isothermal stage, i.e., after reaching the target temperature. All process parameters are summarized in Fig. 1b.

2.3. Characterization methods

The density was measured geometrically and using Archimedes principle according to EN 1389:2003 [21]. The geometrical density was calculated by dividing the sample mass, measured with 0.1 mg accuracy, by the volume as follows: $\rho_{geom} = \frac{m}{\pi \bullet r^2 \bullet h}$, where m is the sample mass, r is the radius and h is the thickness of the pellet. Geometrical density was evaluated for samples with open porosity, while Archimedes method was used for dense samples with no open porosity, using ethanol as the immersion liquid. Relative densities are calculated as follows: $\rho_{rel} = \frac{\rho_{measured}}{\rho_{theoretical}}$, where $\rho_{theoretical}$ is the theoretical density of ZnO which was taken as 5.61 g/cm^3 [22].

The general microstructure was revealed by a field emission scanning electron microscope (Thermo Scientific™ Apreo 2 SEM) on fracture surfaces coated with 5 nm of iridium using a sputter coater (Leica EM ACE600 sputter coater). Average grain size was evaluated by measuring at least 700 grains. The detailed investigation of the microstructure was conducted using a (scanning) transmission electron microscopy (Talos X, FEI) equipped with SuperX EDS detector. The TEM specimen was prepared by focused ion beam (Scios 2, FEI).

Fourier transform infrared spectroscopy (FTIR) was conducted on powders of cold sintered samples to identify any functional groups formed by the interaction between the transient liquid phase and ZnO. The measurements were carried out through attenuated total reflection (ATR) sampling geometry. The spectra were collected using a FT-IR spectrometer (Bruker Vertex 70) in the mid-IR spectral range (4000–500 cm^{-1}) with a resolution of 5 cm^{-1}. The amount of residual organic content in the samples after CSP was determined by thermogravimetric analysis (TGA) using a thermal analyser (Netzsch STA 449 F3 Jupiter®). The measurements were performed under nitrogen atmosphere between 20 and 600 °C with a heating rate of 5 °C/min.

2.4. Mechanical testing and fractography

The biaxial strength of samples cold sintered with acetic and formic acid was measured using the-ball-on-three-balls (B3B) test [23]. In the B3B test setup, the sample is supported in the fixture by three balls on one side and the other side is centrally loaded by a fourth ball. All balls had a diameter of 9 mm, giving a support radius of 5.2 mm. The tests

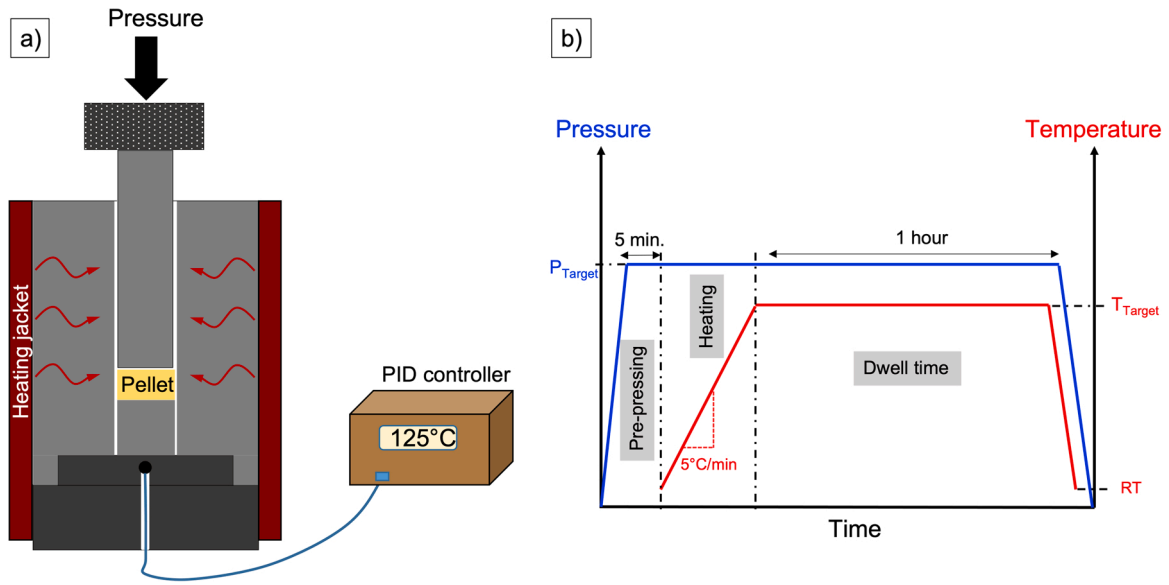

Fig. 1. Experimental setup of the cold sintering process: (a) sintering die wrapped with a heating jacket and connected to a temperature controller through a thermocouple inserted in the bottom base plate, (b) temperature and pressure profile over time during CSP.

were conducted using a universal testing machine (Model C43, MTS® criterion electromechanical test systems) equipped with a 1 kN load cell. All samples were tested in air at ambient conditions (~22 °C and ~20 % relative humidity). The test starts by applying a preload of 5 N to ensure contact between the balls and the sample. Then, the load is increased with a displacement rate of 0.5 mm/min until fracture of the specimen. The force at which fracture occurs is registered and used for stress calculation. The strength was evaluated by calculating the maximum stress endured by the sample, which occurs in the center of the tensile loaded side, using the following equation [23]:

$$\sigma_{\max} = f\left(\frac{R_a}{R}, \frac{t}{R}, \upsilon\right) \bullet \frac{F}{t^2} \quad (1)$$

Where F is the maximum load at fracture, t is the thickness of the pellet and f is a dimensionless factor that depends on the loading and specimen geometry and Poisson's ratio (υ) of the material. R_a is the support radius and R is the specimen radius. For a specimen thickness of 1.4 mm and a Poisson's ratio of 0.34 for ZnO [24], the factor f is approximately 2. The characteristic strength (σ_0) was evaluated by fitting the data according to the two-parameter Weibull statistics using the maximum likelihood method [25,26].

Fractographic analyses were conducted on selected samples fractured in the B3B-tests to identify fracture origins and their location. Assessing fracture origins is important for revealing the underlying reason for the different fracture behaviour of the different set of samples. The fracture surfaces were gold coated using an Agrar sputter coater and observed under a SEM (JEOL JCM- 6000Plus, NeoscopeTM, JEOL Ltd., Tokyo, Japan). The size and location of critical defects were measured on SEM images using an image analysis software (Olympus stream motion).

3. Results and discussion

3.1. Density evolution

Zinc oxide pellets were cold sintered over a temperature range between room temperature and 250 °C using three different aqueous solutions of: formic, acetic, and citric acid. Density trends over various cold sintering temperatures for all liquid phases are shown in Fig. 2. At room temperature, the relative density of all samples is below 75 %. This indicates that the temperature is too low for driving densification

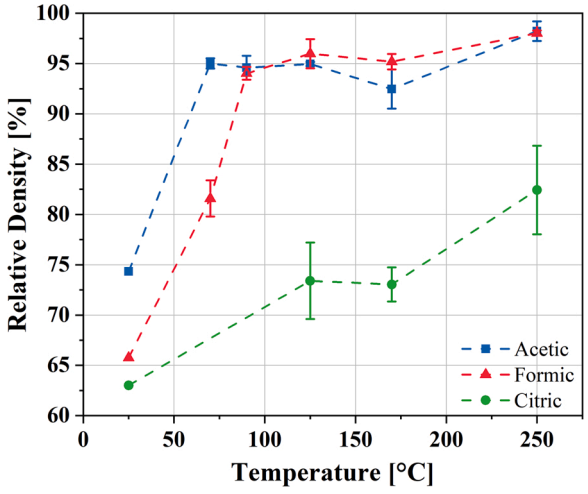

Fig. 2. Relative density as a function of cold sintering temperature for pellets densified using aqueous solutions of acetic, formic, and citric acid, respectively. Error bars represent one standard deviation.

mechanisms and the density is only given by powder compaction and particle rearrangement, favored by the liquid phase. In the case of samples sintered with acetic acid solution, the density increased significantly with small temperature increase, reaching a plateau of ~ 95 % at 70 °C. This trend is in agreement with previous studies on ZnO cold sintered with acetic acid [14,19] with a slight difference in the temperatures, which can be explained by the different heating rates, molarity of the used solution and/or location of the thermocouple in the CSP setup. A similar trend is observed for samples sintered using formic acid, but shifted to higher temperatures, such that a relative density > 95 % was obtained above 90 °C. Both formic and acetic acid sintered samples reached a density of ~ 98 % at 250 °C. However, sintering at temperatures above 170 °C resulted in structurally fragile samples. Citric acid showed the poorest densification behaviour among all liquid phases, with the lowest density at room temperature, thus indicating poor lubrication and rearrangement process. The highest density achieved with this liquid phase was in average 82 % at 250 °C.

3.2. Microstructure evolution

Understanding the densification behaviour requires characterizing microstructural changes during cold sintering at different temperatures. The selection of the temperature of interest was based upon in-situ measurement of the shrinkage during non-isothermal heating to 250 °C using the extensometer attached to the semi-automated press, as described in the experimental section.

Fig. 3a displays the shrinkage curve measured during CSP using acetic acid and its first derivative, which describes the rate of shrinkage. As can be seen, densification starts at a temperature of ~50 °C and ends around 125 °C. The maximum densification rate occurs at ~ 85 °C and is likely to be related to the evaporation of the liquid phase. The microstructure after sintering at 70 °C (Fig. 3b) consists of rounded grains. Such a pronounce morphological change from the prismatic particle shape of the starting powder (Fig. S1b) indicates the activation of the dissolution step, which is absent when pure water is used as a liquid phase as shown in the supplemental information in Fig. S1. Cold sintering at 125 °C (Fig. 3c) results in grain growth from ~67 nm at 70 °C to ~133 nm with faceted grain shape. Sintering at a temperature of 170 °C (Fig. 3d) leads to further grain growth to ~155 nm. However, it is noteworthy that the samples become very fragile at such elevated temperatures. The relative density at all three temperatures (70 °C, 125 °C and 170 °C) was ≥ 93 % after 1 h dwell time. Grain growth of ZnO in presence of zinc acetate under CSP has been proposed to occur via epitaxial growth, Ostwald ripening and/or oriented attachment [27].

For formic acid, compaction of the sample starts to increase around 50 °C and ends at 170 °C during heating, as depicted by the shrinkage and compaction rate curve in Fig. 4a. The maximum shrinkage rate is observed to occur between 85 °C and 100 °C and may be related to the accelerated evaporation of the liquid phase. The microstructure of samples sintered at 70 °C (Fig. 4b) shows spherical grains in the same size range of the starting powder and with significant amount of porosity, which is in good agreement with the measured density of ≤ 83 %. The shape change of the ZnO particles indicates effective dissolution activity of formic acid; however, 70 °C seems to be low to fully drive the densification mechanism. Sintering at 125 °C enhanced the relative density to values above 90 % and lead to the formation of well bound multifaceted grains without coarsening (Fig. 4c). At a higher temperature of 170 °C, no increase in density was achieved. The microstructure is similar to that of samples sintered at 125 °C, consisting of faceted grains (Fig. 4d). An important observation is the preservation of grain size despite the temperature increase to 170 °C, in contrast to the grain growth observed when cold sintering was carried out using acetic acid (Fig. 3c-d). This result demonstrates that grain growth observed under CSP conditions is not only controlled by temperature and time, but also by the type of transient liquid phase. Accordingly, cold sintering using formic acid offers an additional advantage of densifying ZnO to almost full density ~98 %, while maintaining the size of the initial nanometric particles.

Fig. 5a shows the compaction of samples using citric acid and its rate during heating up to 250 °C. The compaction increased with temperature until 220 °C, where a reduction in the displacement along with a negative compaction rate was recorded (upward movement of the pressing piston). This may be explained by pressure build-up in the sample due to water evaporation and decomposition of organics. Morphological change of the starting powder is indicative of the

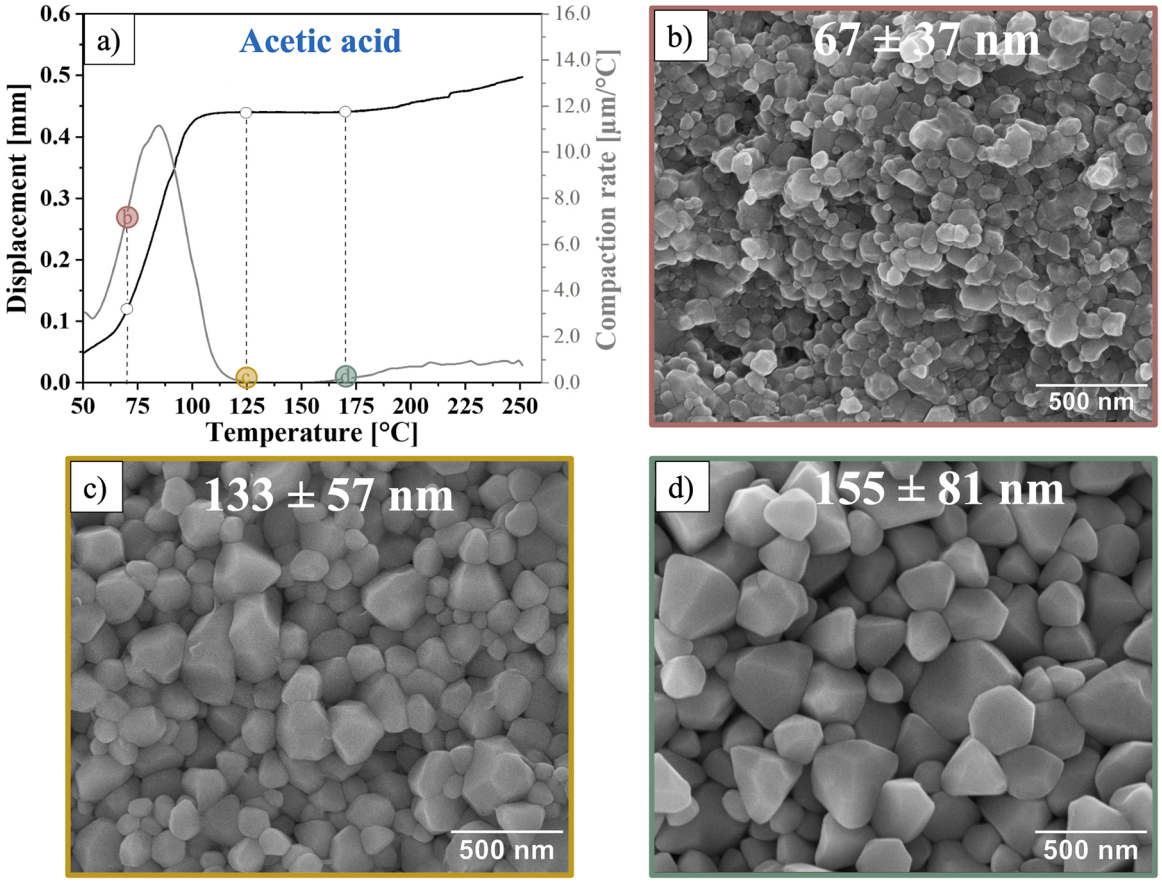

Fig. 3. a) Linear shrinkage during heating to 250 °C (anisothermal) in CSP of ZnO under a pressure of 335 MPa using 2 mol/L acetic acid as a transient liquid phase, the grey curve represents the first derivative of the displacement curve. Microstructure of ZnO cold sintered for 1 h at a temperature of b) 70 °C, c) 125 °C and d) 170 °C. The inset in b, c, and d) shows average grain size ± one standard deviation.

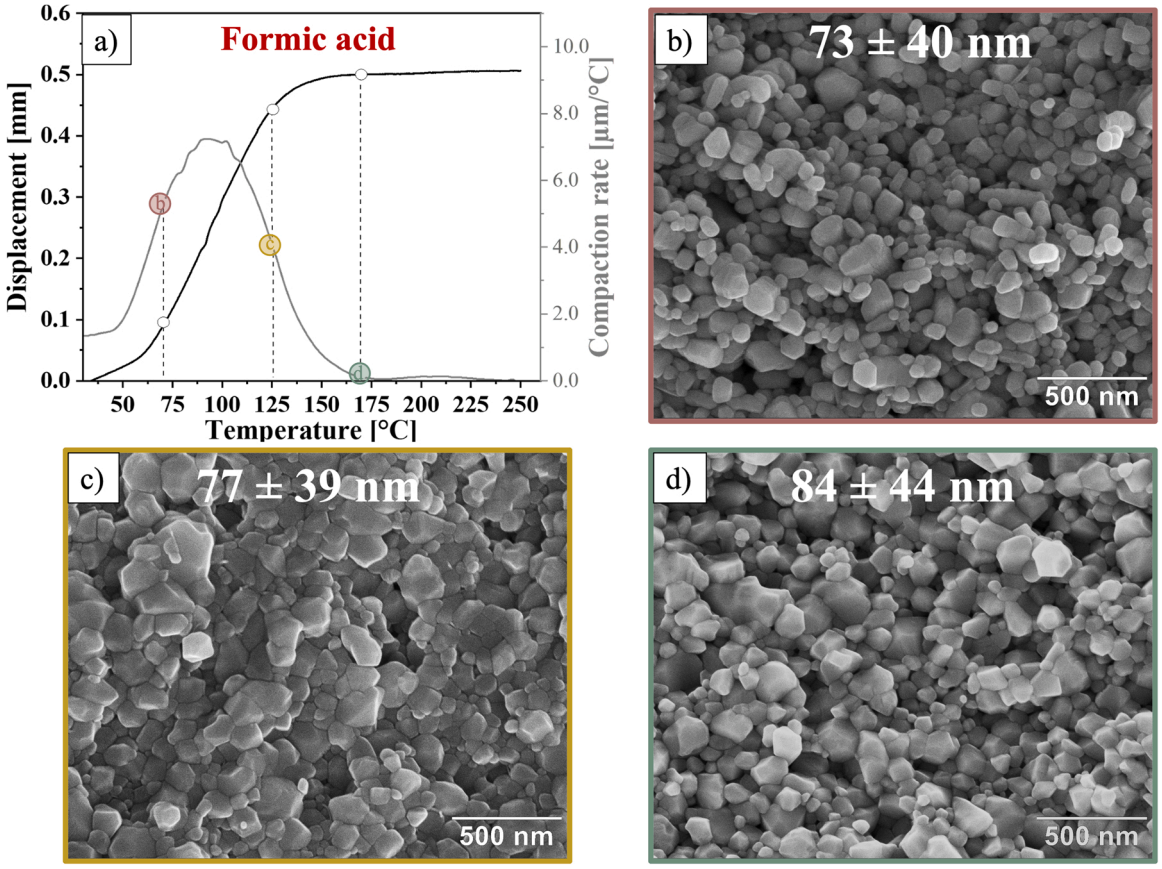

Fig. 4. a) Linear shrinkage during heating to 250 °C (anisothermal) in CSP of ZnO under a pressure of 335 MPa using 2 mol/L formic acid as a transient liquid phase, the grey curve represents the first derivative of the displacement curve. Microstructure of ZnO cold sintered for 1 h at a temperature of b) 70 °C, c) 125 °C and d) 170 °C. The inset in b, c, and d) shows average grain size ± one standard deviation.

dissolution process, it can be observed in the microstructures of samples cold sintered at 125 °C and 170 °C (Fig. 5b-c). At 250 °C (Fig. 5d), grain faceting and large amounts of coarsening occur, but low densification was obtained. As a result, citric acid is not an advisable liquid phase for CSP of ZnO at these conditions, as the relative density of samples sintered with citric acid for 1 h at 250 °C is below 85 %. For the sake of comparison, samples were cold sintered with deionized water within the same temperature range (Fig. S1). As shown in the supplementary data, the powder does not change in morphology and thereby the shrinkage curve corresponds to particle rearrangement and pressure driven compaction without diffusional sintering process.

3.3. Chemical interactions

Densification mechanisms acting in CSP are still under debate, but most studies on cold sintering refer to pressure solution creep as the main sintering mechanism [10]. It is described as a three-stage process: (i) dissolution of the solid phase into the liquid phase, which is enhanced by the external pressure; (ii) diffusion of dissolved ionic species (Zn^{2+} in ZnO systems) in the direction of low chemical potential, i.e. from highly stressed particle–particle contact areas to particles interstitials (pores), and (iii) precipitation of ionic species from the supersaturated solution that evolves during liquid phase evaporation. Hence, unsuccessful densification under CSP can be attributed to the inactivation of any of these stages, and the kinetics are controlled by the lower rate (limiting step) of these serial processes. In the following, the different steps are discussed from chemical point of view, to serve as a guide for selecting appropriate transient solvents.

Step (i): for the dissolution of the solid phase into the liquid phase, the reaction of zinc oxide with the organic acids can be generalized as follows:

$$HX_{(aq)} + H_2O_{(l)} \rightleftharpoons H_3O^+_{(aq)} + X^-_{(aq)} \quad (2)$$

$$ZnO_{(s)} + 2\,H_3O^+_{(aq)} \rightleftharpoons Zn^{2+}_{(aq)} + 3H_2O_{(l)} \quad (3)$$

$$Zn^{2+}_{(aq)} + 2X^-_{(aq)} \rightleftharpoons ZnX_{2(aq)} \quad (4)$$

$$2HX_{(aq)} + ZnO_{(s)} + H_2O_{(l)} \rightleftharpoons ZnX_{2(aq)} + 2H_2O_{(l)} \quad (5)$$

Where HX and X- represent the protonated and deprotonated form of the corresponding organic acid, respectively. As can be seen from Eq. (2), the formation of Zn^{2+} ions is dependent on the pH. Experimental evidence has shown that the dissolution of ZnO at high temperatures is more favourable as the pH value is shifted from 7 [28]. When ZnO is dissolved in the liquid phase, Zn^{2+} rarely exist as free cations and they undergo speciation, which is mainly controlled by the pH and ligands of the liquid phase. In a solution with organic acids, a chelating reaction occurs between the ligands in the acidic liquid phase and Zn^{2+} ions, resulting in the formation of zinc complexes, according to Eq. (3). The formation of complexes with Zn^{2+} ions decreases their concentration in the solution, which further increases the solubility of the zinc oxide. From the three transient solvents selected in this study, citric acid is the only one with a large complex formation constant. This means that the interaction and ligation of the citrate anions with the zinc cations will be significant compared to the relatively small amounts of complexes that are formed for acetic and formic acid, associated with their low formation constants (Table 1). The interaction of the counter anions in solution while dissolving zinc oxide has been previously studied, showing significant increase in solubility based on the interacting anions with zinc oxide [29]. Likewise, citric acid has been demonstrated to be an excellent acid to extract zinc ions from the oxide into solution. Taking

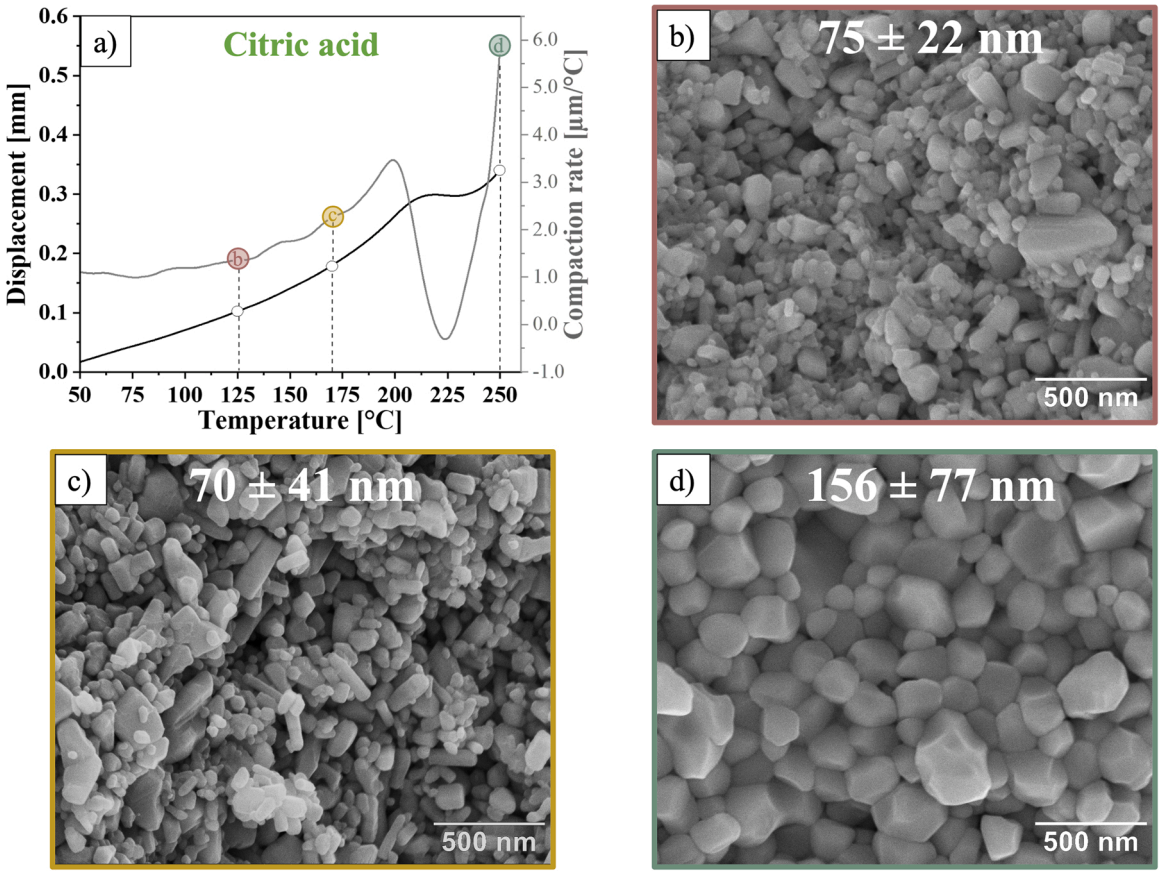

Fig. 5. a) Linear shrinkage during heating to 250 °C (anisothermal) in CSP of ZnO under a pressure of 335 MPa using 2 mol/L citric acid as a transient liquid phase, the grey curve represents the first derivative of the displacement curve. Microstructure of ZnO cold sintered for 1 h at a temperature of b) 125 °C, c) 170 °C and d) 250 °C. The inset in b, c and d) shows the average grain size ± one standard deviation.

Table 1
Chemical constants of zinc complexes formed by formic, acetic, and citric acid reaction with ZnO.

Zinc Carboxylate	Formation constant, Log k_1	Acid pKa	Solubility [g/100 g]	Acid Decomposition Temperature [°C]	Complex Decomposition Temperature [°C]
Zinc Formate	0.73 [30]	3.76 [31]	5.2 [32]	70 [33]	240–260 [34]
Zinc Acetate	0.88 [30]	4.76 [31]	40 [35]	230 [36]	240–271 [37]
Zinc Citrate	4.93 [30]	3.13 [31]	40 [35]	165 [38]	300–400 [39]

this into account, along with the pKa of each acid (Table 1) which dictates the acidity of the solution, the solubility of zinc oxide would be highest in citric acid as it has the lowest pH and the highest complex formation constant.

Step (ii): the diffusion of the aqueous species can be ignored, as the limiting factor is likely to be either the dissolution or the precipitation of ZnO.

Step (iii): the precipitation of the zinc ions into the pores can be further divided into a series of chemically important steps. The first step is the reverse of Eq. (4), where the zinc in the complex needs to be released before the zinc ion can be incorporated into the zinc oxide structure. This means that a higher complex formation constant leads to lower deposition rates. In this regard, citric acid clearly has the largest disadvantage and formic and acetic acid will dissociate faster from the complex. Second, as the water evaporates, the concentration of ions in solution increases until the solution becomes supersaturated, which forces the precipitation of salts. The solubility of zinc formate at 5.2 g/100 g [32] is significantly lower than that of zinc acetate and zinc citrate at 40.0 g/100 g [35] for both, by almost an order of magnitude. As a result, the complex formed by the formate anion and the zinc cation will more readily precipitate while there is enough solvent in the system to be distributed homogeneously around the particles, rather than when there are low amounts of liquid. This could potentially lead to a better densification of the material as the nucleation sites for zinc oxide are better distributed throughout the material and in the triple points, as observed in the TEM images after cold sintering at different temperatures (Fig. 6). Moreover, the early precipitation of zinc formate consumes the amount of ionic species that could be available for coarsening (for example by epitaxial growth [27]) as observed in ZnO systems with zinc acetate. This observation may explain the preservation of the grain size during the densification process. The absence of early nucleation in other organic acids offers higher amounts of ionic species in the system that could take part in the coarsening process, hence affecting the average grain size.

Fig. 6a shows TEM imaging after cold sintering at 70 °C. A low-density microstructure can be observed, which is in good agreement with the 82 % relative density of the sample. For comparison, the microstructure of a sample sintered at 125 °C with a relative density of 95 % is shown in Fig. 6b, displaying a dense microstructure with a small amount of porosity. Fig. 6c and d show EDS maps of samples sintered at 70 °C and 125 °C, respectively. The accumulation of the organic liquid phase at the surface of free grains can be observed, indicating dynamic

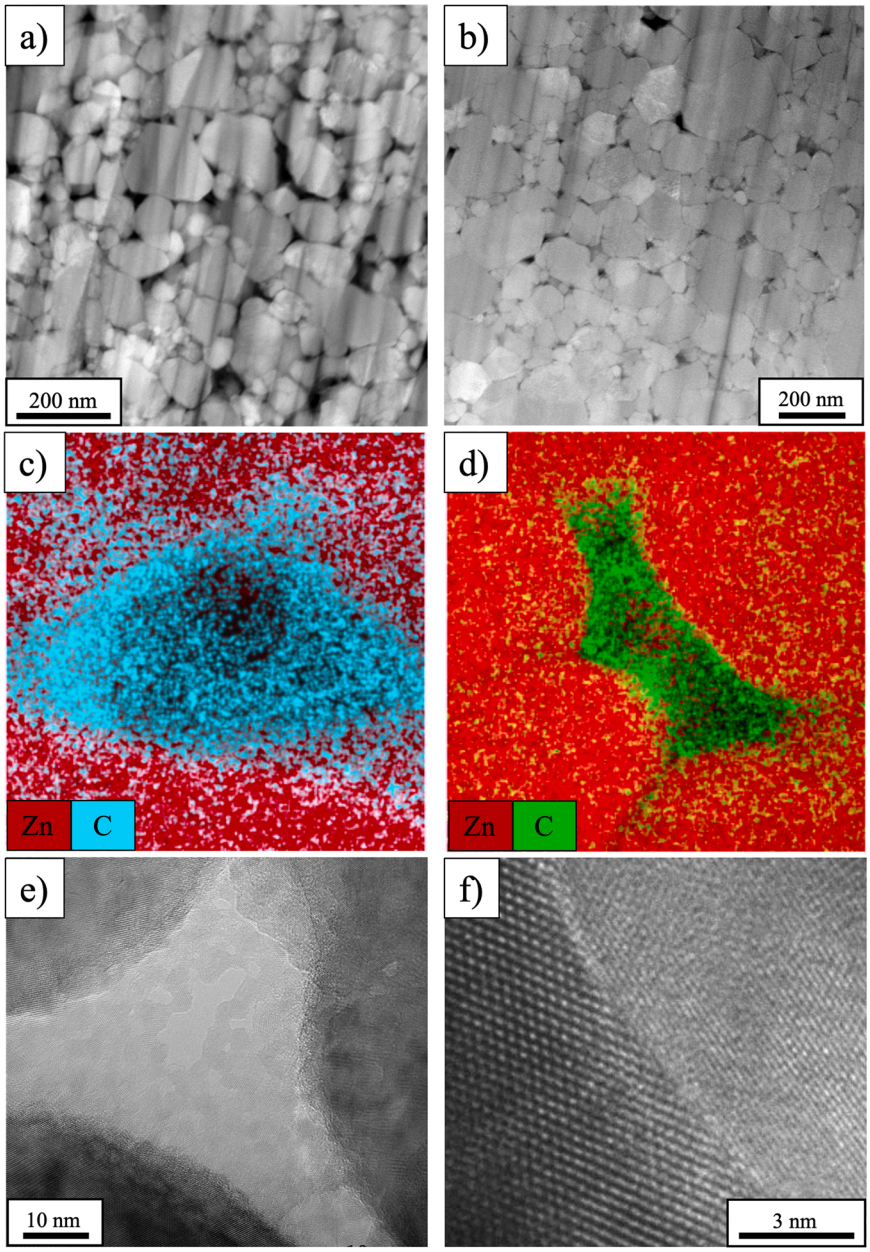

Fig. 6. TEM imaging of the microstructure of samples cold sintered with formic acid at (a,c,e) 70 °C and (b,d,f) at 125 °C. a) low magnification scanning transmission electron microscope (STEM) image of a sample with a relative density of 82 %, b) STEM of a sample cold sintered at 125 °C with a relative density of 95 %, c) EDS mapping of a pore at 70 °C, d) EDS map of pore at 125 °C, note the nucleation of ZnO in the pore, e) high magnification TEM at a junction between 3 grains (no carbon detected by EDS) and f) high magnification TEM of a grain boundary after cold sintering at 125 °C. The stripes in a) and b) are artefacts induced by the focused-ion beam milling process (curtaining).

interaction between formic acid and ZnO, which is important for the chelating reactions. The depletion of the organic phase in the centre of the pores could be ascribed to the nucleation of new ZnO, as observed in Fig. 6d and e. This is contrasted with previous and current observations of cold sintering with acetic acid, where no nucleation was observed [40]. A clean grain boundary between two neighboring grains is shown in Fig. 6f. It is also worth noting that no amorphous phase was observed, demonstrating complete recrystallization.

To reveal the chemisorption of formic acid onto the ZnO surface, FTIR spectroscopy was conducted on pure ZnO (as a reference), ZnO powder mixed with formic acid (prior to CSP) and on a sample cold sintered at 125 °C (Fig. 7a). The broad band between 3000 and 3600 cm^{-1} is characteristic for absorption frequency of –OH stretching mode [41], which indicates humidity capture and surface hydroxylation, as observed in the pure powder and the powder mixed with formic acid. This peak diminishes after cold sintering at 125 °C which indicates the evaporation of the liquid phase, in accordance with intended purpose of the liquid phase to be transient in CSP. Typical FTIR spectrum of pure formic acid exhibits a characteristic peak at 1750 cm^{-1}, which is related to the vibration frequency of the carbonyl group ($C = O$) [42]. This peak splits into two peaks that are related to the symmetric and antisymmetric stretching of the carboxyl group (COO^-), when it is coordinating to a metal. At room temperature (RT), the spectrum is similar to that of zinc formate [43] (peaks at 1583 cm^{-1} and the three neighboring peaks at 1398, 1378 and 1354 cm^{-1}), indicating that formic acid already starts to dissolve ZnO at RT and forms zinc formate species. Moreover, the peaks are in good agreement with the calculated spectrum by Lenz et al. [44], suggesting a bridging bidentate structure. After cold sintering at 125 °C the characteristic peaks of zinc formate disappeared; an indication for the decomposition of the zinc formate complex and the formation of adsorbed formate species. The shifting of the symmetric stretching frequency of the carboxyl group (COO^-) from 1583 cm^{-1} (at RT) to 1571 cm^{-1} (at 125 °C) has been previously observed by Buchholz et al. [45] and was attributed to the coordination of residual adsorbed formate species onto ZnO in a quasi-bidentate configuration. This shows the dynamic coordination character of formic acid, making it a good

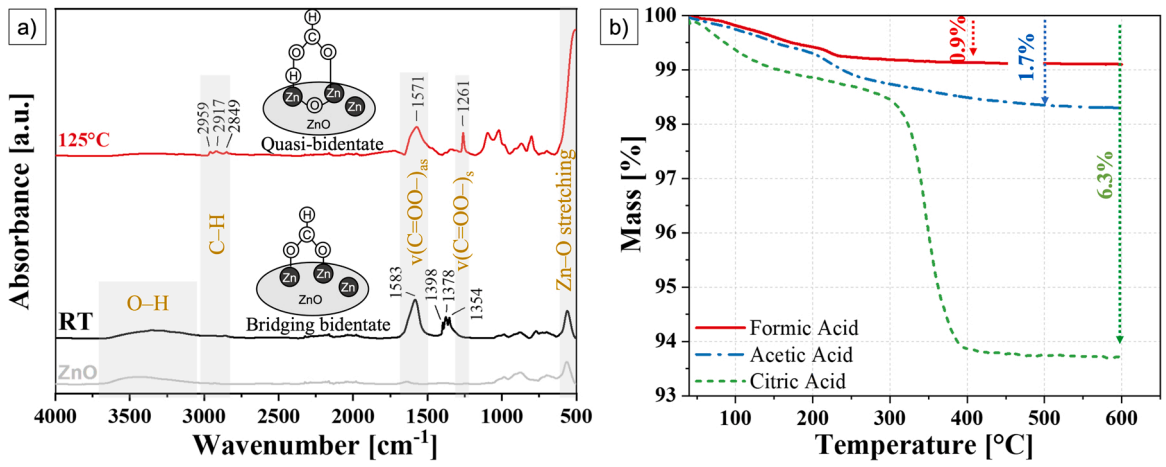

Fig. 7. a) FTIR of ZnO, ZnO impregnated with 2 M solution of formic acid, and ZnO sintered with formic acid at 125 °C. b) TGA showing the weight loss of cold sintered samples at 125 °C using formic, acetic, and citric acid. The inset schematics in figure a) displays the coordination geometry of formic acid on ZnO.

chelating agent– a property targeted in CSP. FTIR spectra for acetic and citric acid liquid phases has been discussed in the literature elsewhere [40,46]. These were measured in this study and are shown in Figs. S2 and S3 in the supplementary information.

The decomposition of the formed complexes is a necessary step for densification and removal of residual organics, which could negatively affect electrical [9] and mechanical properties [47]. The decomposition of organics can take various routes. In general terms, organic acids, HX, and organometallic salts, ZnX_2, can thermally decompose into different species such as CO, CO_2, H_2, H_2O. Formic acid has been reported to adsorb onto zinc oxide both as full HCOOH molecule and $HCOO^-$ ion at temperatures below 100 °C [49]. It has also been shown that there is significant decomposition of formic acid starting at 70 °C [33], with formate ions being catalytically decomposed on most surfaces [48], including that of zinc oxide [49]. On the other hand, acetic and citric acid have a much higher decomposition temperature of 230 °C [36] and 165 °C [38], respectively. The low decomposition temperature of formic acid facilitates its decomposition and the reprecipitation of zinc oxide. Furthermore, the decomposition temperatures of the formed salts with formic acid are lower than those formed with citric and acetic acid (Table 1). As a result, the combination of low decomposition temperatures, low solubility of the salt, and low complex formation constants makes formic acid the best choice among these acids to sinter zinc oxide.

Fig. 7b illustrates the corresponding TGA curves, showing small amounts of residual liquid phase content for samples sintered with formic acid (~0.9 %) and acetic acid (~1.7 %), compared to that of citric acid (~6.3 %). Weight losses up to 200 °C are attributed to the loss of bound water and dehydration of zinc carboxylates. The weight loss of 0.31 % and 1.0 % at ~230 °C for formic and acetic acid, respectively, is associated with the decomposition of residual organics. In the citric acid sample, the decomposition of citrate complexes was observed between 300 °C and 400 °C with a weight loss of 5.1 %. It is expected for citric acid to have a higher organic content (greater mass loss during TGA analysis) as it has a relatively high decomposition temperature and a complex decomposition path to various organic molecules [38]. On the other hand, formic and acetic acid are both simplest organic acids, and their decomposition should leave little room for organic reactions, in particular for formic acid being the simplest of the two. It is still noteworthy that both acetic and formic acid hold such low organic concentrations after sintering for only 1 h.

3.4. Mechanical response

Fig. 8 shows individual failure stresses as well as the characteristic strength of each series of samples cold sintered using acetic acid and formic acid, and is compared to samples sintered with zinc acetate [50]. For samples cold sintered using acetic acid, a characteristic strength of σ_0= 42 (36–48) MPa and a Weibull modulus of m = 5 (3–7) were measured, where the bracketed values correspond to the 90 % confidence intervals. This strength value is relatively low compared to the results of samples cold sintered using formic acid, where a characteristic strength of σ_0= 88 (83–94) MPa and m = 8 (5–11) were obtained. The strength results measured on samples sintered with formic acid show a ~40 % higher strength than previously reported values on cold sintered ZnO using zinc acetate (σ_0= 64 (62–67) MPa and m = 8 (6–10)) [50]. It is also noteworthy that this study on cold sintering using formic acid is preliminary and does not represent an upper limit for the strength, since the processing parameters used in this work have not been optimized. However, it shows the potential of enhancing the structural integrity of cold sintered materials by selecting an appropriate transient liquid phase.

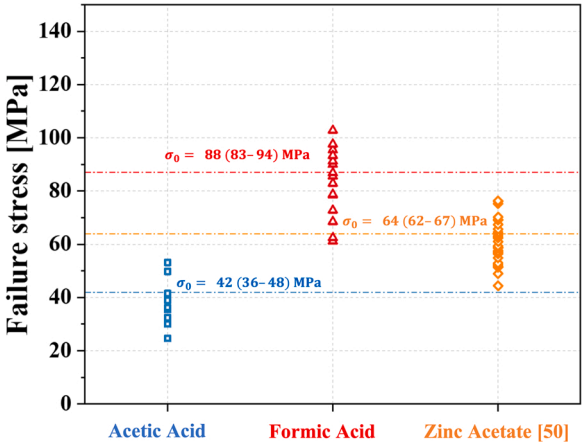

Fig. 8. Biaxial fracture stress distributions for cold sintered samples using aqueous solutions of acetic acid, formic acid, and zinc acetate. The characteristic strength, σ_0, and the corresponding 90 % confidence interval is inserted for each set. The failure stress values of specimens cold sintered using zinc acetate were taken from the work of Lowum et al. [50].

In order to understand the reason for the remarkable difference in the strength of samples cold sintered using acetic acid and formic acid, a fractographic analysis was conducted. Fig. 9a and b show fracture surfaces and typical defects observed in samples densified with acetic acid and formic acid solutions. In samples densified using acetic acid (Fig. 9a), fracture originates typically from delaminated regions in the

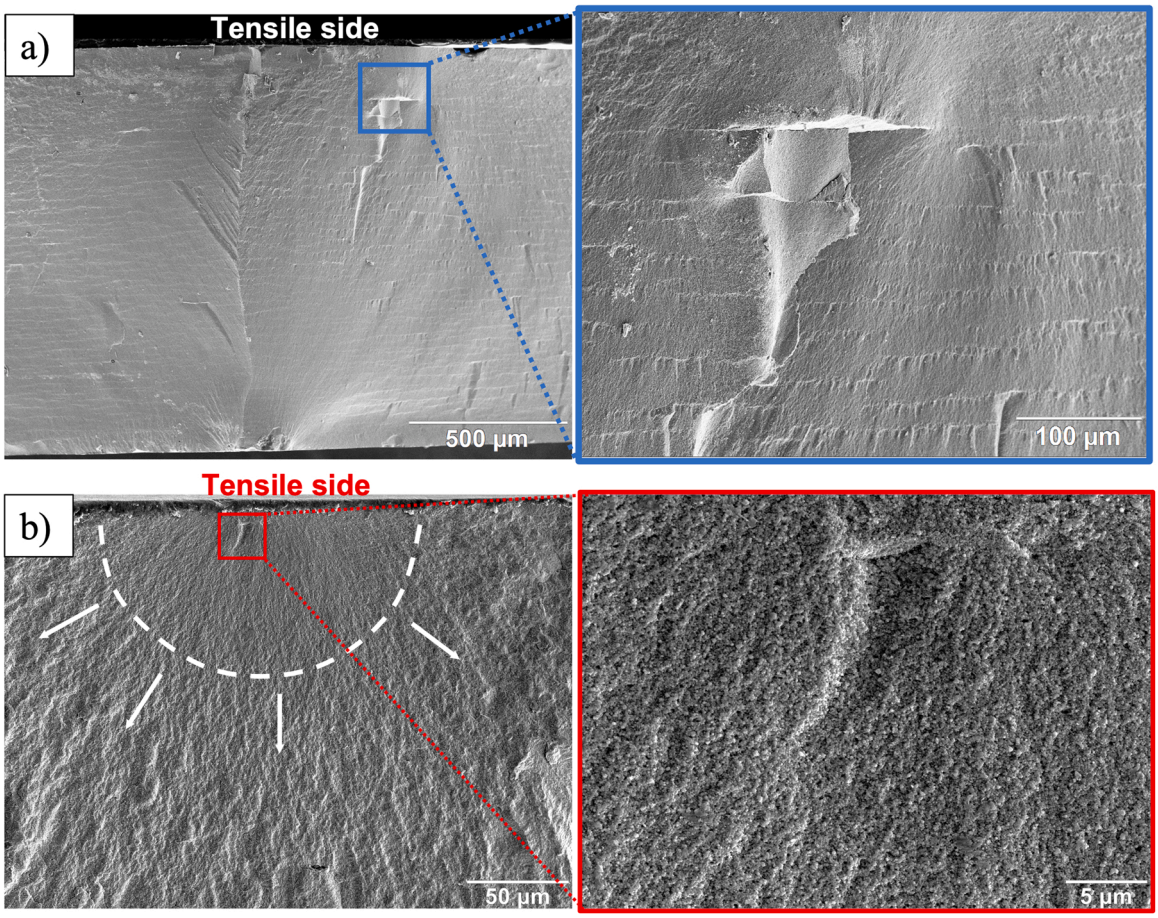

Fig. 9. Fracture surfaces and enlarged view of fracture origins in: a) sample cold sintered with acetic acid solution with a failure stress of 36 MPa. The fracture origin is a delaminated area in the subsurface. b) cold sintered with formic acid solution with a failure stress of 91 MPa. The fracture origin is identified as a near-surface flaw. The white dashed line and arrows highlight the fracture mirror and Hackle lines, respectively.

microstructure. In addition, the fracture surface shows striation-like features oriented horizontally and perpendicular to the direction of pressure application, which may act as potential delamination sites and stress concentrators. This may explain the lower strength and larger scatter in the strength values (lower Weibull modulus). The occurrence of such delaminations could be attributed to anisotropic effects due to a combined action of pressure and acetic acid–ZnO interaction, for example, preferred growth of ZnO grains in the [0001]-direction in presence of zinc acetate as shown by Dargatz et al. [27]. However, no sound conclusions can be drawn, and further investigation is needed.

In the case of samples densified using formic acid, surface or near-surface defects were found as fracture origin, as commonly encountered in dense ceramics sintered under conventional methods. In some cases, volume defects associated with non-uniform liquid phase distribution, and hence, densification were identified as fracture origins. Fig. 9b shows a typical fracture surface after B3B testing of a sample densified using formic acid, where the failure originated from a flaw (crack) near the surface. Compared to samples densified with acetic acid, formic acid results in a homogeneous microstructure with fracture surfaces showing features (e.g. fracture mirror, hackle lines) as on a well densified material. It may be hypothesized that the superior mechanical performance achieved with formic acid could be associated with a better grain boundary cohesion. However, fracture toughness measurements are required to verify this hypothesis and will be undertaken in future work.

In summary, it has been demonstrated that the type of liquid phase used in CSP has an influence on the densification and mechanical strength of the cold sintered material. While various liquid phases may yield high densities, the mechanical strength may not be guaranteed as shown in the case of ZnO densified with acetic acid solution. The selection of formic acid as a transient liquid phase for CSP is a first step toward enhancing the reliability of cold sintered samples as shown in this work. Optimization of the processing parameters and reduction of processing induced defects, such as delamination and non-uniform densification, by controlling thermal and pressure gradients will be investigated in future work.

4. Conclusions

Cold sintering of ZnO to relative densities above 95 % at temperatures below 125 °C using 2 mol/L aqueous solutions of formic acid and acetic acid is demonstrated. Compared to densification using acetic acid, where significant grain growth was observed, samples densified using formic acid retain their grain size over all temperature regimes and relative densities. Microstructural observation based on TEM analyses show that densification using formic acid can be driven by precipitation and nucleation of new ZnO grains in pore regions which maintains the grain size. This is the first instance of this behaviour being observed and it is not observed during sintering using acetic or citric acid. The importance of the precipitation step for driving densification is demonstrated by a comparative study using acetic and citric acid. Even though a higher dissolution rate of ZnO in citric acid is expected, poor densification was obtained. This is explained by the high formation constant, high solubility of the zinc citrate complex, and high thermal stability of citric acid, which impede the precipitation step. In contrast, zinc formate and zinc acetate complexes have much lower formation

constants which allows the release of Zn^{2+} ions. Additionally, formic acid has a low thermal stability and solubility of the salt compared to acetic and citric acid, leading to faster precipitation and high densification under CSP. Despite the similar densities for formic and acetic acid samples, the biaxial characteristic strength of samples cold sintered using formic acid was twice that of acetic acid sintered samples and is about 40 % higher than the previously reported strength in the literature using zinc acetate. This highlights the chemical complexities that are important to consider when selecting a transient solvent for CSP, as it can affect the mechanical performance. This study proposes formic acid as a more favourable liquid phase for CSP and represents a first step toward optimizing the mechanical reliability of cold sintered materials.

Declaration of Competing Interest

The authors declare that they have no known competing financial interests or personal relationships that could have appeared to influence the work reported in this paper.

Acknowledgements

Funding for this research was provided by the European Research Council (ERC) excellent science grant "CERATEXT" through the Horizon 2020 program under contract 817615. Abdullah Jabr acknowledges the Austrian Marshall Plan Foundation for the financial support during his stay at Penn State university. All authors would like to thank the Material Research Institute and its Materials Characterization Laboratory and the staff for help in the state-of-the-art experimental facilities used in this study. Julian Fanghanel is grateful for partial support from the NSF DMR-1729634. Clive Randall would like to thank NSF_FMSG (2134643) and AFOSR (FA 9550-19-1 0372) for partial support of this work and for supporting experimental costs of the work for all students and postdoctoral researchers.

Appendix A. Supporting information

Supplementary data associated with this article can be found in the online version at doi:10.1016/j.jeurceramsoc.2022.11.071.

References

[1] M.N. Rahaman, Sintering of Ceramics, Taylor & Francis, 2008.
[2] J.D. Katz, Microwave sintering of ceramics, Annu. Rev. Mater. Sci. 22 (1992) 153–170, https://doi.org/10.1146/annurev.ms.22.080192.001101.
[3] H.V. Atkinson, S. Davies, Fundamental aspects of hot isostatic pressing: an overview, Met. Mat. Trans. A 31 (2000) 2981–3000, https://doi.org/10.1007/s11661-000-0078-2.
[4] Z. Zhao, V. Buscaglia, P. Bowen, M. Nygren, Spark plasma sintering of nanocrystalline ceramics, KEM 264–268 (2004) 2297–2300, https://doi.org/10.4028/www.scientific.net/KEM.264-268.2297.
[5] R.M. German, P. Suri, S.J. Park, Review: liquid phase sintering, J. Mater. Sci. 44 (2009) 1–39, https://doi.org/10.1007/s10853-008-3008-0.
[6] H. Guo, J. Guo, A. Baker, C.A. Randall, Hydrothermal-assisted cold sintering process: a new guidance for low-temperature ceramic sintering, ACS Appl. Mater. Interfaces 8 (2016) 20909–20915, https://doi.org/10.1021/acsami.6b07481.
[7] H. Guo, A. Baker, J. Guo, C.A. Randall, Protocol for ultralow-temperature ceramic sintering: an integration of nanotechnology and the cold sintering process, ACS Nano 10 (2016) 10606–10614, https://doi.org/10.1021/acsnano.6b03800.
[8] J.-P. Maria, X. Kang, R.D. Floyd, E.C. Dickey, H. Guo, J. Guo, A. Baker, S. Funihashi, C.A. Randall, Cold sintering: current status and prospects, J. Mater. Res. 32 (2017) 3205–3218, https://doi.org/10.1557/jmr.2017.262.
[9] S. Funahashi, J. Guo, H. Guo, K. Wang, A.L. Baker, K. Shiratsuyu, C.A. Randall, Demonstration of the cold sintering process study for the densification and grain growth of ZnO ceramics, J. Am. Ceram. Soc. 100 (2017) 546–553, https://doi.org/10.1111/jace.14617.
[10] A. Ndayishimiye, S.H. Bang, ChristopherJ. Spiers, C.A. Randall, Reassessing cold sintering in the framework of pressure solution theory (S095522192200749X). J. Eur. Ceram. Soc. (2022) https://doi.org/10.1016/j.jeurceramsoc.2022.09.053.
[11] X. Zhao, J. Guo, K. Wang, T. Herisson De Beauvoir, B. Li, C.A. Randall, Introducing a ZnO–PTFE (Polymer) nanocomposite varistor via the cold sintering process, Adv. Eng. Mater. 20 (2018), 1700902, https://doi.org/10.1002/adem.201700902.
[12] J. Guo, X. Zhao, T.H.D. Beauvoir, J.-H. Seo, S.S. Berbano, A.L. Baker, C. Azina, C. A. Randall, Recent progress in applications of the cold sintering process for ceramic–polymer composites, Adv. Funct. Mater. 28 (2018), 1801724, https://doi.org/10.1002/adfm.201801724.
[13] S. Dursun, K. Tsuji, S.H. Bang, A. Ndayishimiye, C.A. Randall, A route towards fabrication of functional ceramic/polymer nanocomposite devices using the cold sintering process, ACS Appl. Electron. Mater. 2 (2020) 1917–1924, https://doi.org/10.1021/acsaelm.0c00225.
[14] X. Kang, R. Floyd, S. Lowum, M. Cabral, E. Dickey, J. Maria, Mechanism studies of hydrothermal cold sintering of zinc oxide at near room temperature, J. Am. Ceram. Soc. 102 (2019) 4459–4469, https://doi.org/10.1111/jace.16340.
[15] M.Y. Sengul, J. Guo, C.A. Randall, A.C.T. vanDuin, Water-mediated surface diffusion mechanism enables the cold sintering process: a combined computational and experimental study, Angew. Chem. Int. Ed. 58 (2019) 12420–12424, https://doi.org/10.1002/anie.201904738.
[16] R.D. Floyd, S. Lowum, J.-P. Maria, Cold sintering zinc oxide with a crystalline zinc acetate dihydrate mass transport phase, J. Mater. Sci. 55 (2020) 15117–15129, https://doi.org/10.1007/s10853-020-05100-9.
[17] J. Gonzalez-Julian, K. Neuhaus, M. Bernemann, J. Pereira da Silva, A. Laptev, M. Bram, O. Guillon, Unveiling the mechanisms of cold sintering of ZnO at 250 °C by varying applied stress and characterizing grain boundaries by Kelvin Probe Force Microscopy, Acta Mater. 144 (2018) 116–128, https://doi.org/10.1016/j.actamat.2017.10.055.
[18] A. Ndayishimiye, Z. Fan, S. Funahashi, C.A. Randall, Assessment of the role of speciation during cold sintering of ZnO using chelates, Inorg. Chem. 60 (2021) 13453–13460, https://doi.org/10.1021/acs.inorgchem.1c01806.
[19] S.H. Bang, A. Ndayishimiye, C.A. Randall, Anisothermal densification kinetics of the cold sintering process below 150 °C, J. Mater. Chem. C 8 (2020) 5668–5672, https://doi.org/10.1039/D0TC00395F.
[20] R. Floyd, S. Lowum, J.-P. Maria, Instrumentation for automated and quantitative low temperature compaction and sintering, Rev. Sci. Instrum. 90 (2019), 055104, https://doi.org/10.1063/1.5094040.
[21] E. Standards, BS EN 1389:2003 Advanced Technical Ceramics-Ceramic Composites-Physical Properties-Determination of Density and Apparent Porosity. Https://Www.En-Standard.Eu. (n.d.). www.en-standard.eu/bs-en-1389–2003-advanced-technical-ceramics-ceramic-composites-physical-properties-determination-of-density-and-apparent-porosity/.
[22] PubChem, Zinc Oxide, (n.d.). ⟨https://pubchem.ncbi.nlm.nih.gov/compound/14806⟩. (Accessed 18 August 2022).
[23] A. Börger, P. Supancic, R. Danzer, The ball on three balls test for strength testing of brittle discs: stress distribution in the disc, J. Eur. Ceram. Soc. 22 (2002) 1425–1436, https://doi.org/10.1016/S0955-2219(01)00458-7.
[24] H.N. Yoshimura, A.L. Molisani, N.E. Narita, J.L.A. Manholetti, J.M. Cavenaghi, Mechanical properties and microstructure of zinc oxide varistor ceramics, MSF 530–531 (2006) 408–413, https://doi.org/10.4028/www.scientific.net/MSF.530-531.408.
[25] W. Weibull, A statistical distribution function of wide applicability, J. Appl. Mech. 18 (1951) 253.
[26] Advanced Technical Ceramics - Monolithic Ceramics - Mechanical Tests at Room Temperature - Part 5: Statistical Analysis, (1997).
[27] B. Dargatz, J. Gonzalez-Julian, O. Guillon, Anomalous coarsening of nanocrystalline zinc oxide particles in humid air, J. Cryst. Growth 419 (2015) 69–78, https://doi.org/10.1016/j.jcrysgro.2015.02.101.
[28] P. Benezeth, D.A. Palmer, D.J. Wesolowski, C. Xiao, New measurements of the solubility of zinc oxide from 150 to 350∘C, J. Solut. Chem. (2002) 27.
[29] R. Larba, I. Boukerche, N. Alane, N. Habbache, S. Djerad, L. Tifouti, Citric acid as an alternative lixiviant for zinc oxide dissolution, Hydrometallurgy 134–135 (2013) 117–123, https://doi.org/10.1016/j.hydromet.2013.02.002.
[30] D.R. Burgess, NIST SRD 46. Critically Selected Stability Constants of Metal Complexes: Version 8.0 for Windows, (2004). https://doi.org/10.18434/M32154.
[31] D.R. Lide, CRC Handbook of Chemistry and Physics, eighty fouth ed., J. Am. Chem. Soc. 126 (2004) 1586–1586. https://doi.org/10.1021/ja0336372.
[32] C. Balarew, T.P. Dirkse, O.A. Golubchikov, M. Salomon, C. Balarew, O. A. Golubchikov, T.P. Dirkse, S. Trendafilova, S. Tepavitcharova, T. Ageyeva, P. Baldini, G. D'Andrea, IUPAC-NIST solubility data series. 73. Metal and ammonium formate systems, J. Phys. Chem. Ref. Data 30 (2001) 1–163, https://doi.org/10.1063/1.1354207.
[33] H.N. Barham, L.W. Clark, The decomposition of formic acid at low temperatures, ACS Publ. (2002), https://doi.org/10.1021/ja01154a042.
[34] P. Mars, J.F. Scholten, P. Zwietering, The Catalytic Decomposition of Formic Acid, (n.d.) 79.
[35] B. Granum, Opinion of the Scientific Committee on Consumer safety (SCCS) – final opinion on water-soluble zinc salts used in oral hygiene products, Regul. Toxicol. Pharmacol. 99 (2018) 249–250, https://doi.org/10.1016/j.yrtph.2018.09.007.
[36] Y. Li, S. Zhou, J. Li, Y. Ma, K. Chen, Y. Wu, Y. Zhang, Experimental study of the decomposition of acetic acid under conditions relevant to deep reservoirs, Appl. Geochem. 84 (2017) 306–313, https://doi.org/10.1016/j.apgeochem.2017.07.013.
[37] A.V. Ghule, K. Ghule, C.-Y. Chen, W.-Y. Chen, S.-H. Tzing, H. Chang, Y.-C. Ling, In situ thermo-TOF-SIMS study of thermal decomposition of zinc acetate dihydrate, J. Mass Spectrom. 39 (2004) 1202–1208, https://doi.org/10.1002/jms.721.
[38] M.M. Barbooti, D.A. Al-Sammerrai, Thermal decomposition of citric acid, Thermochim. Acta 98 (1986) 119–126, https://doi.org/10.1016/0040-6031(86)87081-2.
[39] A. Srivastava, V.G. Gunjikar, A.P.B. Sinha, Thermoanalytical studies of zinc citrate, bismuth citrate and calcium citrate, Thermochim. Acta 117 (1987) 201–217, https://doi.org/10.1016/0040-6031(87)88115-7.

[40] S.H. Bang, M.Y. Sengul, Z. Fan, A. Ndayishimiye, A.C.T. van Duin, C.A. Randall, Morphological and chemical evolution of transient interfaces during zinc oxide cold sintering process, Mater. Today Chem. 24 (2022), 100925, https://doi.org/10.1016/j.mtchem.2022.100925.
[41] G. Xiong, U. Pal, J.G. Serrano, K.B. Ucer, R.T. Williams, Photoluminesence and FTIR study of ZnO nanoparticles: the impurity and defect perspective, Phys. Status Solidi C. 3 (2006) 3577–3581, https://doi.org/10.1002/pssc.200672164.
[42] Formic acid, NIST Chemistry WebBook, SRD 69. (n.d.). ⟨https://webbook.nist.gov/cgi/cbook.cgi?ID=C64186&Type=IR-SPEC&Index=1⟩. (Accessed 5 October 2022).
[43] Zinc formate - Optional [ATR-IR] - Spectrum - SpectraBase, John Wiley & Sons, Inc. SpectraBase. (n.d.). ⟨https://spectrabase.com/spectrum/HYtTZ2m3fuI⟩. (Accessed 5 October 2022).
[44] A. Lenz, L. Selegård, F. Söderlind, A. Larsson, P.O. Holtz, K. Uvdal, L. Ojamäe, P.-O. Käll, ZnO nanoparticles functionalized with organic acids: an experimental and quantum-chemical study, J. Phys. Chem. C 113 (2009) 17332–17341, https://doi.org/10.1021/jp905481v.
[45] M. Buchholz, Q. Li, H. Noei, A. Nefedov, Y. Wang, M. Muhler, K. Fink, C. Wöll, The interaction of formic acid with zinc oxide: a combined experimental and theoretical study on single crystal and powder samples, Top. Catal. 58 (2015) 174–183, https://doi.org/10.1007/s11244-014-0356-7.
[46] S.P. Pasilis, J.E. Pemberton, Spectroscopic investigation of uranyl(VI) and citrate coadsorption to Al2O3, Geochim. Cosmochim. Acta 72 (2008) 277–287, https://doi.org/10.1016/j.gca.2007.09.036.
[47] K. Nur, M. Zubair, J.S.K.-L. Gibson, S. Sandlöbes-Haut, J. Mayer, M. Bram, O. Guillon, Mechanical properties of cold sintered ZnO investigated by nanoindentation and micro-pillar testing, J. Eur. Ceram. Soc. 42 (2022) 512–524, https://doi.org/10.1016/j.jeurceramsoc.2021.10.011.
[48] W.L. Nelson, C.J. Engelder, The thermal decomposition of formic acid, J. Phys. Chem. 30 (1926) 470–475, https://doi.org/10.1021/j150262a003.
[49] T. Kondo, T. Ogawa, K. Kishi, K. Hirota, Formic acid decomposition on zinc oxide by use of Oxygen-18 Tracer*, Z. Für Phys. Chem. 67 (1969) 284–290, https://doi.org/10.1524/zpch.1969.67.4_6.284.
[50] S. Lowum, R. Floyd, R. Bermejo, J.-P. Maria, Mechanical strength of cold-sintered zinc oxide under biaxial bending, J. Mater. Sci. 54 (2019) 4518–4522, https://doi.org/10.1007/s10853-018-3173-8.